




DIGITAL RECONSTRUCTION OF HISTORIC ROOF STRUCTURES: DEVELOPING A WORKFLOW FOR A HIGHLY AUTOMATED ANALYSIS

RECONSTRUCCIÓN DIGITAL DE ESTRUCTURAS DE TEJADOS HISTÓRICOS: DESARROLLO DE UN FLUJO DE TRABAJO DE ANÁLISIS ALTAMENTE AUTOMATIZADO

Markus Pöchtrager^{a,b,*}, Gudrun Styhler-Aydın^a, Marina Döring-Williams^a, Norbert Pfeifer^b 

^a Institute of History of Art, Building Archaeology and Restoration, TU Wien, Karlsplatz 13/E251, 1040 Vienna, Austria.
markus.poechtrager@tuwien.ac.at; gudrun.styhler@tuwien.ac.at; marina.doering-williams@tuwien.ac.at

^b Department of Geodesy and Geoinformation, TU Wien, Gußhausstraße 27-29/E120, 1040 Vienna, Austria.
norbert.pfeifer@geo.tuwien.ac.at

Highlights:

- This article presents a novel approach to automated reconstruction of beam structures by modelling geometry from segmented point clouds.
- Wooden beams are modelled as cuboids, thus a rectangular cross-section with minor deformation is required.
- An accuracy of less than 1 cm can be reached for modelled beams, compared to the reference LiDAR point cloud.

Abstract:

Planning on adaptive reuse, maintenance and restoration of historic timber structures requires extensive architectural and structural analysis of the actual condition. Current methods for a modelling of roof constructions consist of several manual steps including the time-consuming dimensional modelling. The continuous development of terrestrial laser scanners increases the accuracy, comfort and speed of the surveying work in roof constructions. Resulting point clouds enable detailed visualisation of the constructions represented by single points or polygonal meshes, but in fact do not contain information about the structural system and the beam elements. The developed workflow contains several processing steps on the point cloud dataset. The most important among them are the normal vector computation, the segmentation of points to extract planar faces, a classification of planar segments to detect the beam side faces and finally the parametric modelling of the beams on the basis of classified segments. This enables a highly automated transition from raw point cloud data to a geometric model containing beams of the structural system. The geometric model, as well as additional information about the structural properties of involved wooden beams and their joints, is necessary input for a further structural modelling of timber constructions. The results of the workflow confirm that the proposed methods work well for beams with a rectangular cross-section and minor deformations. Scan shadows and occlusion of beams by additional installations or interlocking beams decreases the modelling performance, but in general a high level of accuracy and completeness is achieved at a high degree of automation.

Keywords: historical timber structures; LiDAR (Light Detection And Ranging); point clouds; digital reconstruction; beam frame

Resumen:

Las estructuras históricas de madera requieren un análisis arquitectónico y estructural exhaustivo de su condición real en aras de planificar la reutilización flexible, el mantenimiento y la restauración. Los métodos actuales que modelan las construcciones de cubiertas pasan por aplicar varias etapas en modo manual, que incluye el lento modelado dimensional. El desarrollo continuo de escáneres láser terrestres aumenta la exactitud, la comodidad y la velocidad del trabajo topográfico en construcciones de tejados. Las nubes de puntos resultantes permiten la visualización detallada de las construcciones representadas por puntos o mallas poligonales, pero de hecho no contienen información sobre el sistema estructural y los elementos del travesaño. El flujo de trabajo desarrollado contiene varias etapas de procesamiento en el conjunto de datos de la nube de puntos. Los más importantes son el cálculo del vector normal, la segmentación de puntos que extraen caras planas, la clasificación de segmentos planos que detectan las caras laterales del travesaño y, finalmente, el modelado paramétrico de los travesaños en función de los segmentos clasificados. Esto permite una transición altamente automatizada de los datos de la nube de puntos brutos a un modelo geométrico que contiene los travesaños del sistema estructural. El modelo geométrico, así como la información adicional sobre las propiedades estructurales de las vigas de madera involucradas y de sus juntas, es información necesaria de entrada para el modelado estructural eventual de las construcciones de madera. Los resultados del flujo de trabajo confirman que los métodos propuestos funcionan bien en travesaños que presentan secciones transversales rectangulares y deformaciones menores. Las sombras en los escaneados y las oclusiones de los travesaños a partir de instalaciones adicionales o vigas

* Corresponding author: Markus Pöchtrager, markus.poechtrager@tuwien.ac.at



entrelazados disminuye el rendimiento del modelado, pero en general se logra un nivel de exactitud e integridad elevado con un alto grado de automatización.

Palabras clave: estructuras históricas de madera; LiDAR (*Light Detection And Ranging*); nubes de puntos; reconstrucción digital; travesaño

1. Introduction

Surveying buildings is still challenging for historic timber structures for which detailed documentation and deformation-accurate maps are needed. Above all, the process is labour-intensive, although historic wooden roof structures feature regular and repetitive constructions, composed of linear elements. They are, however, complex with reference to their specific geometrical arrangement and the different joints between the beams. Surveying methods in use today combine traditional manual and modern, automated surveying techniques including hand-measurement with tapes, total station measurement (tachymetry), as well as three-dimensional (3D) laser scanning.

Surveys of wooden roof structures are required in a number of cases, including i) planning an adaptive re-use of unused attic lofts, ii) protecting monuments on the basis of sustainable preservation strategies, and iii) calculating and verifying resource-friendly and efficiently structural consolidation. Depending on the specific application, the surveys provide 2D and 3D digital models as well as drawings, including i) deformation-accurate sets of plans showing the current status, ii) digital models of the structure, iii) information about individual joints, iv) a reconstruction of the assembly process and, e.g., construction phases, v) carpenters' marks, and vi) the position of dendrochronological samples. Additionally, the so-called catalogue of rafters provides detailed information on all (sub-) assemblies including the joints, in the form of a systematic description of all geometrical and mechanical features of the roof structure (see Fig. 1).

ii) degradation due to moisture, and iii) displacement of joints (Eßer, Styhler-Aydın, & Hochreiner, 2016a; Eßer, Styhler-Aydın, & Hochreiner, 2016b).

Currently, a detailed and accurate modelling of roof constructions comprises a number of consecutive steps. Firstly, terrestrial laser scanning (TLS) is performed at multiple scan positions to capture the entire scene. Typically, several scan positions are necessary to capture all details, because of the scan shadow objects in the foreground occlude the surfaces behind. Secondly, the orientation (i.e. position and angular attitude) for the different TLS point clouds from the individual scan positions has to be determined. This can be performed accurately and reliably with artificial targets visible in multiple scans. Thirdly, 2D slices in the point cloud are selected manually, following the roof structure. Finally, dimensional modelling is performed on the basis of these 2D slices for each pair of rafters. However, each of these steps and therefore the entire method is very labour intensive.

Laser scanning, also termed LiDAR (Light Detection And Ranging), is an accurate, fast and highly automated surveying technique. Within minutes a highly detailed point cloud describing the scene from the scanner point of view is obtained and provided in the scanner coordinate system. For the principles and methods of laser scanning see Vosselman & Maas (2010). Using either tie points (e.g. artificial targets) or the surfaces of the scanned objects, multiple scans can be transformed into a superior coordinate system, as described by Glira, Pfeifer, Briese, & Ressler (2015) and Besl & McKay (1992). The combined 3D point cloud covers all surfaces, and thus objects, which are visible from the laser scanner positions, with a dense set of points. For historic roof structures, exhibiting confined space and therefore short measurement ranges, a few points are typically measured per 1 cm². Correspondingly, the distance between neighbouring points is in the order of mm to cm. Obviously, beams, their axes and the joints are not directly obtained by laser scanning, but they are implicitly contained in the raw 3D point cloud.

An efficient transformation of the 3D point cloud of TLS to a data format suitable for architectural modelling and analysis like in the catalogue of rafters and structural assessment with an analysis of the acting forces is still missing. We propose a new method for the automatic derivation of the linear elements of historic timber roof structures from raw TLS point clouds. It exploits the high density of TLS point clouds. The new method will be demonstrated for different historic timber roof structures of the Vienna Imperial Palace (Wiener Hofburg).

First ideas for the automated parametric modelling approach have already been described in Pöchtrager, Styhler-Aydın, Döring-Williams, & Pfeifer (2017) and are updated and extended by more recent work results in this paper.

2. Problem statement and related work

The various applications for the architectural and structural analysis of existing roof structures define

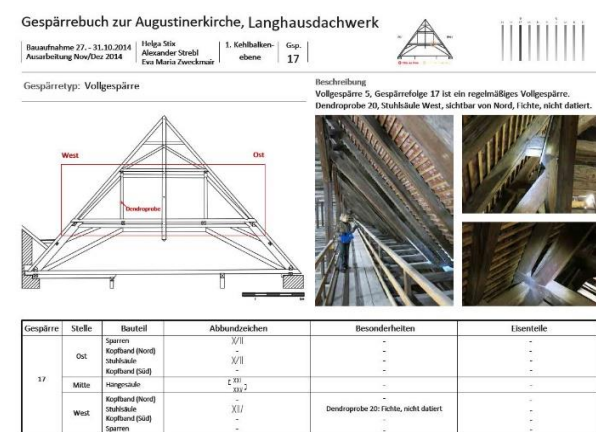


Figure 1: Section of the catalogue of rafters of the Augustinian Church, Vienna Imperial Palace (© H. Stix, A. Strebl, E.M. Zweckmair, all TU Wien, 2014). The main graph shows the typical cross-section of a full pair of rafters. It is complemented by photos, an overview plan, and a table of exceptions.

Recently Hochreiner, Eßer, & Styhler-Aydın (2016) have extended the approach described above towards structural assessment. Numerical structural models are built on the basis of the architectural survey data. This process, however, requires information beyond standard architectural documentation, such as i) the allocation of crack formations due to shrinkage,

requirements in terms of the nature and quality of the digital roof structure reconstruction. For architectural documentation, we expect a survey accuracy of 1 cm, which reflects a scale of 1:50 in the deformation-accurate plan record.

In order to plan the adaptive re-use of a roof, it is necessary to model the forces acting on the beams. Thus, a model composed of beam axes and joints has to be derived. Together with the beam dimensions, the nature of the joints, and parameters of the beam material, the forces present in the roof structure can be determined. This is the basis for planning adaptation to the structure.

Both architectural documentation and extraction of beam axes require a very high degree of completeness. Thus, manual additions and corrections on the result of the automated processing will be inevitable, in order to guarantee the completeness of the final model. Incomplete models arise generally from bad scan quality, from scan shadow areas or if beams are occluded by further installations. To get a correct and complete model, the separation of relevant (e.g. beam) and irrelevant (e.g. floor) objects needs to be well-considered. The automated classification of relevant beam objects gets more reliable with the definition of minimum and maximum beam dimensions and the integration of overall structural information (e.g. repetition of rafters).

Based on our needs the aim is to develop a set of methods and corresponding tools for an automated processing of point clouds derived from laser scanning. Requirements for an automation can be formulated for the measurement and for the object. It is assumed that the point clouds are dense (e.g. distance of neighbouring points below 5 mm). Typical laser scanning accuracy of, e.g., 2 mm, is assumed for the standard deviation of each point (coordinate direction). For the modelling of the objects, it is technically required to have at least two adjacent side faces of a beam represented in the point cloud. This also implies that the beam faces share a common edge. Additionally, it is assumed that the beams are straight (i.e. not bent) and have a rectangular cross-section. Slight bending of beams can be handled and checked with the use of threshold values.

Related work in the sense of automatic surface reconstruction using unorganised point sets was carried out in the last decades by Hoppe, DeRose, Duchamp, McDonald, & Stuetzle (1992), Attene & Spagnuolo (2000) and Kazhdan, Bolitho, & Hoppe (2006). The aim is always to find an interpolating or approximating surface through all points, e.g. in the form of a TIN (Triangular Irregular Network). Some of the approaches provide an oriented 2D manifold, i.e. a surface for which "inside" and "outside" can be defined. The combination of tacheometric surveying, laser scanning and images for obtaining the 3D point cloud for applications in the cultural heritage context is described in Dorninger, Nothegger, & Rasztovits (2013). A combination of triangulation and bump mapping is used to represent the surface of a sculpture in local detail. For a more complete picture of available recording and modelling techniques for cultural heritage use cases, see the book by Stylianidis & Remondino (2016).

In contrast to the general surface description, our aim is the reconstruction of individual objects, i.e. beams. Besides the point cloud information, we can integrate overall information on the shape of objects, e.g. minimum and maximum width and length of a beam or the

rectangular cross-section. Symmetry and repetition of objects in the structural system can help to complete the model, even in regions where points were determined sparsely.

Automated architectural analysis based on point clouds have already been developed for several applications, e.g. by (Zhang & Zakhor, 2014) for the classification of window areas. Automation of reconstruction and analysis requires knowing the key features and characteristics of the respective applications. For the modelling of wooden beam structure, the planarity of points is the main feature to detect side faces of beams. The elongated shape of beams and their connectedness suggests considering previous work on piping installations. Approaches for automated reconstruction of piping installations from point clouds have been studied and developed by several authors (Rabbani, Dijkman, Van den Heuvel, & Vosselman, 2007; Lee, Son, Kim, & Kim, 2013). In a first step, the point cloud is split into groups using segmentation, clustering, and/or skeletonization. Then, voting schemes such as Random sample consensus (RANSAC) or the Hough transform are used for the estimation of cylinder parameters, which can be refined using, e.g., least-squares parameter estimation. A cylinder has 5 parameters (4 axis parameters and the radius), but is not confined along its axis. Unless top and bottom surfaces are also covered by points, the first and last points along the axis, respectively, are used to confine the cylinder. In comparison, a beam with a rectangular cross-section has 7 parameters. The problem of the top and bottom surface is the same, but all four sides, pairwise parallel, have to be covered by points in order to reconstruct the cross section. For cylinders, a small surface patch is, in theory, enough to determine its 5 parameters. If the curvature is determined in one point, the direction for the principal curvature with a value of 0 is the direction of generators, while the other principal curvature is the inverse of the radius.

Historic roof structures typically do not exhibit an ideal beam form. Deviations can occur in the form of a more complex cross-section because of the chamfer or an irregular cross section due to timber irregularity, or because of bending in the longitudinal direction. Additionally, cracks occur in timber constructions, which may require more than a geometrical model. A structural analysis of deformed timber structures with geometric mesh modelling and structural finite element modelling (FEM) is shown by Bassier, Hadjidemetriou, Vergauwen, Van Roy, & Verstrynghe (2016). The contribution of Yang, Koehl, & Grussenmeyer (2017) presents a parametric modelling of beams with the rectangular cross-section, which is similar to our approach. However, they use tachymetric measurement to detect the edges of beams manually.

Several related methods for parametric modelling of prismatic objects from point clouds have been developed in recent years. For example, Chida & Masuda (2016) demonstrate the reconstruction of cuboids. In their industrial context, the shapes are more precisely planar. In addition, occlusions appear more frequent in historic roof structures than in Chida & Masuda's examples. Furthermore, end sides are normally not visible in roof constructions, as they occur in the beam joints. Jung et al. (2014) use a similar approach, but suggest concentrating on a semi-automatic method, in which outlines of planar faces are determined automatically, and are used for subsequent manual modelling for the as-built

BIM (Building Information Modelling). Especially the object-oriented modelling of beams and the interaction in their joints give new possibilities for structural and architectural analysis. All available information about our modelled objects can be collected in BIM to facilitate the analysis process. Dore & Murphy (2017) summarise the current state of the art for as-built BIM and HBIM (Historic Building Information Modelling), including modelling concepts and quality control. Baik, Yaagoubi, & Boehm (2015) demonstrate the reconstruction of complex facades using point clouds in a BIM (Autodesk Revit). An overview of “automatic geometry generation from point clouds for BIM” in the context of room walls, windows, and floor are given by Thomson & Boehm (2015), while specific methods are suggested by Xiong, Adan, Akinci, & Huber, (2013).

3. Method

3.1. Overview

For an automated digital reconstruction of roof structures, a new workflow was developed. The aim of the work is to derive structural and architectural models from point clouds recorded by laser scanning. The proposed processing chain (see Fig. 2) therefore starts with a registered point cloud as input data. In the first step of the processing the point cloud is imported into the module-based software OPALS (Pfeifer, Mandlbürger, Otepka, & Karel, 2014). This import stage converts the point cloud into the efficient ODM (OPALS Datamanager) data format, composed of two separated spatial indices, enabling a fast read and write access to point attribute information. ODM stores the point cloud in tiles (Level 0 index), and builds up a k-d tree (Level 1 index) with the points of a tile, when they are accessed. With these data, any operation carried out on the single points can store information in the point attributes. Quick access to point attributes –such as normal vector components and segment ID– is needed in several processing steps in OPALS modules, as well as in the project specific implementation of the workflow stages.

Right after the import step, normal vectors are computed for each point. Normal vectors are estimated for a point by calculating a robust plane for the point and its k-nearest neighbour points. The optimal number of neighbour points k (e.g. 4-16) might depend on the point density. To avoid the selection of points that are too far away, a maximum search radius r_{max} can be specified or estimated from the point density (e.g. 0.05-0.1 m). A detailed discussion on the influence of the neighbourhood size is given in Nothegger & Dorninger (2009).

Based on the normal vectors provided by the module OPALS Normals, the segmentation module can then be used to split the point cloud into segments of neighbouring points that fulfil a local homogeneity criterion. A proper selection of the homogeneity criterion (including normal vector information) enables the detection and planar modelling of side faces of wooden elements or walls as single segments from laser scans. The segments in the point cloud are the main input for the following project-specific processing steps of finding adjacent segments forming one beam and fitting cuboids to the entire point set describing a beam.

For the automatic detection of wooden beams, the segments first need to be categorised into straight beam

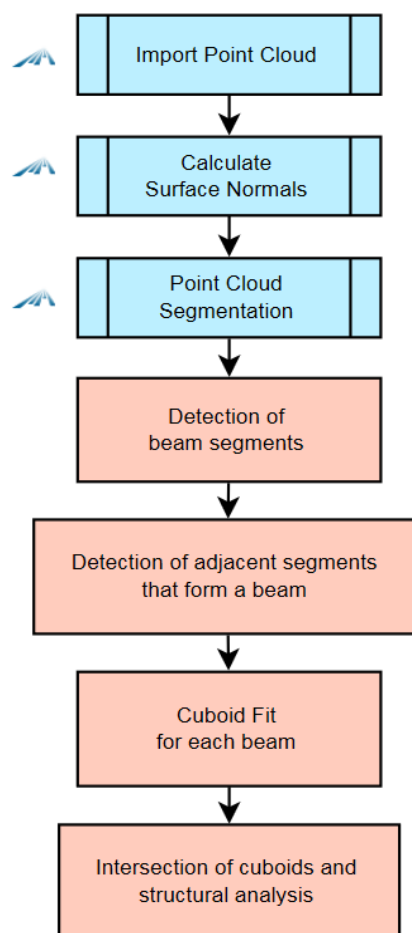


Figure 2: Stages of the processing chain, using OPALS modules (blue) and new routines, implemented in Python (red).

segments and segments of other elements in the construction (e.g. roof tiles, walls, wooden walkways, etc.). It is important to detect as many beam segments as possible and remove all segments of objects that have no relevance for the architectural and structural analysis.

In the next step, classified beam segments need to be connected into adjacent elements that form a beam. For all the points that belong to the same beam, a cuboid can be determined if at least two sides of the beam are covered with segments. This cuboid is the basis for the representation of the beam in the 3D architectural model. As a final step, the cuboids need to be extended and intersected to get the joints in the woodwork as observed in the architectural analysis.

The following sections describe the main processing steps in more detail. While OPALS modules are used for the data import, the calculation of normal vectors and the segmentation, all subsequent steps have been implemented in a Python application, using some functionality of the ODM.

3.2. Segmentation

In the workflow, the normal vector information of each point is the main input parameter for the segmentation. To get the normal vector estimation at a specific point, its neighbour points need to be considered. The selection of the neighbour points has a major influence on the result. To get precise results –especially on the edges of beams– a robust plane fit algorithm for the point and its neighbour points is used. The normal vector of the fitting plane gets

assigned to the point. The nearest neighbour search is based on the full 3D coordinates of the points.

In the segmentation step, two neighbouring points belong to the same segment if the angle between the normal vectors is below some threshold α_{max} (e.g. $4-6^\circ$) and the distance between the points is within a maximum search radius r_{max} (e.g. 0.02-0.05 m). The formula for the local homogeneity in the segments can, therefore, be written as:

$$\cos^{-1}(\vec{n}_p \cdot \vec{n}_n) < \alpha_{max} \quad (1)$$

\vec{n}_p and \vec{n}_n are the unit normal vectors of a segment point and a neighbouring candidate point.

3.3. Identification of beam segments

An automated classification of beam segments was developed (Fig. 3) to recognise the sides of the beams.

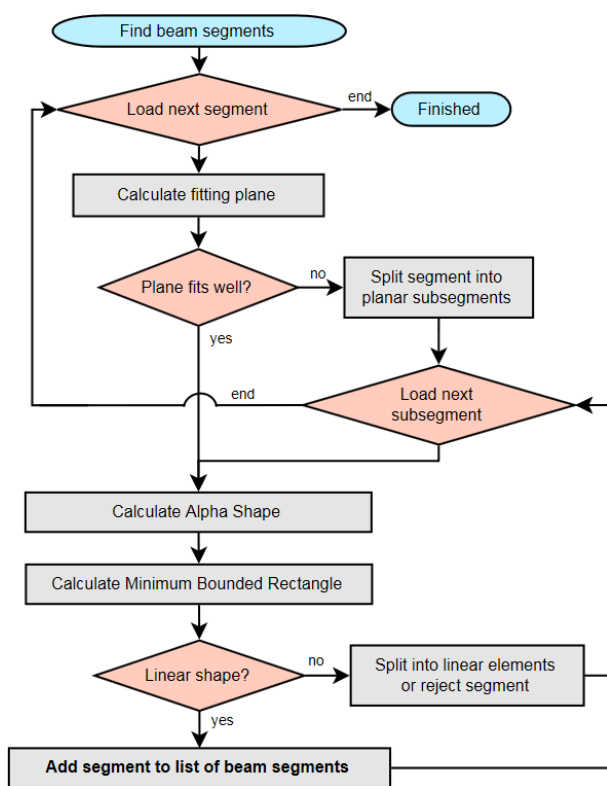


Figure 3: Flowchart of beam segment classification.

The classification is based on two pre-steps, namely i) the detection of planar segments, and ii) the detection of the shape of a segment.

3.3.1. Detection of planar segments

To begin with, a least squares fitting plane is calculated for all points in a segment using principal component analysis. It provides the three eigenvalues of the plane and the fitting root mean square error (RMSE). If the plane fits well according to the RMSE, which implies that the points of the segment are more or less coplanar, the segment can be considered as a flat surface. If no plane model fits all segment points, the segment needs to be split up into planar (sub-) segments. This is achieved by adapting the RANSAC algorithm (Fischler & Bolles, 1981) for plane fitting. This algorithm iteratively detects the largest planar sub-segment of the original segment until no more planar segments can be detected (Fig. 4).

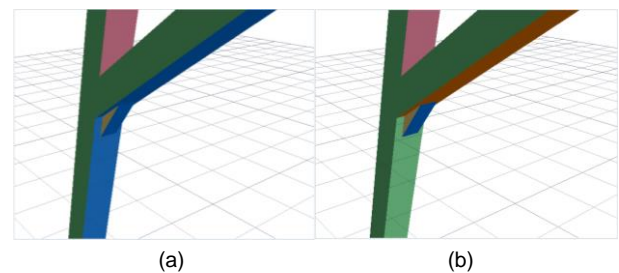


Figure 4: a) Non-planar segments (e.g. connected via bridges) are split up into b) planar (sub-) segments.

3.3.2. Detection of the shape

The next step is to derive information about the shape of planar segments. To get the 2D shape and boundary representation for the points in planar segments, α -shapes were calculated. α -shape computation is closely related to the computation of the convex hull and Delaunay triangulation but in contrast to the convex hull, the polygon does not need to be convex. Additionally, the selection of the alpha value allows the specification of a degree of generalisation for the shape.

In addition to the α -shape, the minimum bounding rotated rectangle (MBR) is calculated. The MBR is a rectangle that contains all points of a segment with a minimum area. α -shapes and MBRs provide essential information about the straightness of segments and thus constitute major input for the classification of segments. Both shape descriptors are shown in Fig 5.

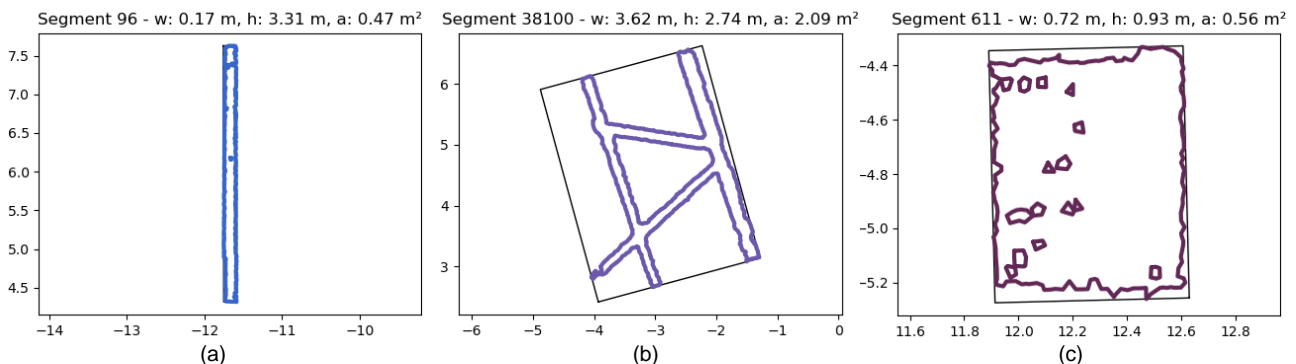


Figure 5: Segment classification based on linear shape. Three classes: a) beam segments; b) separable sub-segments; c) other. The segments are represented by α -shapes (coloured polygons) and minimum bounding rectangles (grey rectangles).

A wide variety of different shape indices or shape factors were investigated for the classification of segments, see e.g. Li, Goodchild, & Church (2013). The workflow we developed in fact only uses two decisive factors, namely:

- Elongation factor:

$$f_{elong} = \sqrt{\frac{\lambda_l}{\lambda_w}} \quad (2)$$

where λ_l and λ_w are the largest and second largest eigenvalues of the plane fit describing length and width of a segment.

- Ratio between the area of α -shape and MBR

$$f_{area} = \frac{A_\alpha}{A_{MBR}} \quad (3)$$

With a combination of these two factors the planar segments can be classified (see Fig. 5) into the following three classes:

- Linear-shaped (straight) segment.
- Non-linear segment with separable sub-segments.
- Non-linear compact segment.

While non-linear compact segments (c) are rejected, the linear-shaped segments (a) are added to the list of beam segments if the beam width is within a given range w_{min} - w_{max} (e.g. 10-40 cm). The segments of the third class (b) can be split up into sub-segments of straight beam segments.

3.4. Identification of adjacent beam segments

Based on the list of segments classified as beam faces, the next task is to detect and join adjacent segments that form together a wooden beam. Segments are considered to belong to the same beam if they meet the following three conditions:

1. Distance between the centroid of segment A and the plane of segment B:

$$|C_A - P_B| < dist_{max} \quad (4)$$

2. Angle between the normal vectors:

$$\cos^{-1}(\vec{n}_A \cdot \vec{n}_B) \approx \left[0, \frac{\pi}{2}, \pi, \frac{3\pi}{2}\right] \quad (5)$$

3. Axes in longitudinal direction are parallel:

$$\cos^{-1}(\vec{l}_A \cdot \vec{l}_B) \approx [0, \pi] \quad (6)$$

\vec{l}_A and \vec{l}_B are the eigenvectors of the largest eigenvalues of the segments A and B.

The threshold of $dist_{max}$ in (4) was chosen to specify the maximum thickness of beams. If two candidate segments are orthogonal, $dist_{max} = w_{max}/2$. If the segments are on opposite beam sides, $dist_{max} = w_{max}$. Equations (5) and (6) allow small deviations from their strict formulation by considering angular thresholds.

If all these conditions are met it is guaranteed that two segments are adjacent, orthogonal or facing each other and they have parallel longitudinal axes that are parallel to their common beam axis as well.

This association of adjacent planar segments can be used to achieve a first rough 3D modelling of beams. If at least two sides of a beam are covered by planar segments, it is possible to even go a step further and fit a rigid body to the segment points.

3.5. Fit cuboids for beams

The associated segments of a beam are processed further, as the workflow contains a stage where attempts are made to fit a cuboid to the points of the beam segments.

The cuboid is a flawless representation of the historic wooden beam. Any deformations of the beams, such as deflection or torsion, are neglected in this first modelling approach. For the fitting of the cuboid, a least squares estimation (LSE) is used. Pairwise orthogonal or parallel planes make up the side faces of the cuboid that are fitted to the points. The squared distances between segment points and the cuboid are minimised with the use of the following four equations for the calculation of the distances to the four side faces:

$$f1(p_{1,j}): (p_{1,j} - p_0)^T \cdot r_1 = d_{1,j} \quad (7a)$$

$$f2(p_{2,j}): (p_{2,j} - p_0)^T \cdot r_2 = d_{2,j} \quad (7b)$$

$$f3(p_{3,j}): (p_{3,j} - (p_0 + a \cdot r_1))^T \cdot r_1 = d_{3,j} \quad (7c)$$

$$f4(p_{4,j}): (p_{4,j} - (p_0 + b \cdot r_2))^T \cdot r_2 = d_{4,j} \quad (7d)$$

$$\text{with } p_0 = CoG + s \cdot r_1 + t \cdot r_2$$

where

$p_{i,j}$ = point j of a side face i ($i = 1, 2, 3, 4$).

$d_{i,j}$ = distance of a point j to its side face i .

r_1, r_2 = axes of the beam coordinate system.

a, b = beam dimensions in r_1 - and r_2 - direction.

CoG = centre of gravity of all beam points.

p_0 = reference (base) point of the beam.

s, t = shift of p_0 from CoG into the beam corner in r_1 - and r_2 - direction.

Equations (7a) to (7d) show, that it is necessary to know to which beam side face a segment belongs. The parameters of the cuboid beam modelling are shown in Fig. 6.

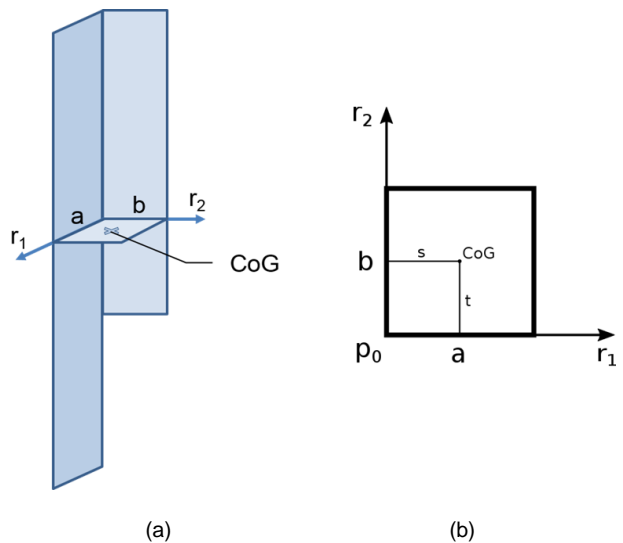


Figure 6: Parameters and settings of the cuboid modelling shown in: a) 3D and b) 2D isometry.

The length of the beam is calculated by projecting the beam points onto the longitudinal axis of the beam coordinate system. The outermost points on the longitudinal axis give the length of the beam.

3.6. Intersect beams and analyse the structure

The difficulties in the final processing stage are the modelling of the beams in their correct dimension as well as the detection and modelling of woodworking joints and how the timber elements interlock. The materials used and the techniques applied in a joint indicate the purpose of that joint within the structure.

Scan shadows and reduced quality in some areas of the point cloud make it impossible to detect all beams, to their full extent automatically. It is, therefore, necessary to extend these incomplete beams to their full length and to the joints where they interlock with other beams.

A semi-automated joint detection –where the user selects two beams that interlock– can be achieved quickly, by a simple calculation of the shortest connecting line of the beam axes. Based on length and orientation of this shortest connecting line segment and the connected beams, the joint type can be classified. If beams get elongated with user guidance, it is important to be aware of the need for a validation, which can be done with general point cloud information.

For a fully automated approach overall information, e.g. about the regularity of the entire roof structure, is indispensable. Knowledge about the repetition of rafters in the structural system can indicate missing beams. Even if the segmentation does not give enough useful information for an automated modelling of beams, the point cloud contains information as to whether there are objects or not. Combination of overall roof structure information and point cloud information could fill the incomplete areas in the model. This part of the workflow is still under development.

For collaboration with structural engineers, the beams and joints need to be exported into a format and data structure they can work with. The STEP data format as described in the ISO 10303-21 ([International Organization for Standardization, 2016](#)) standard is widely used for the representation of 3D objects in computer-aided design and gives a proper framework for a data exchange. A further structural analysis requires the integration of additional material information.

Processing as described in Sections 3.2. to 3.5. has been implemented and evaluated so far. The next section provides an overview of the results of each processing step.

3.7. Results of the processing chain

The results of the normal vector computation for each point are heavily dependent on the selection of neighbour points in the plane estimation and the chosen robust method of dealing with edges. For the robust normal vector estimation in OPALS, eight nearest neighbour points within a maximum distance of 0.09 m have been selected. The resulting normal vectors show homogeneous directions for points on the same beam side face. The robust plane estimation prevents edges being rounded (Fig. 7).

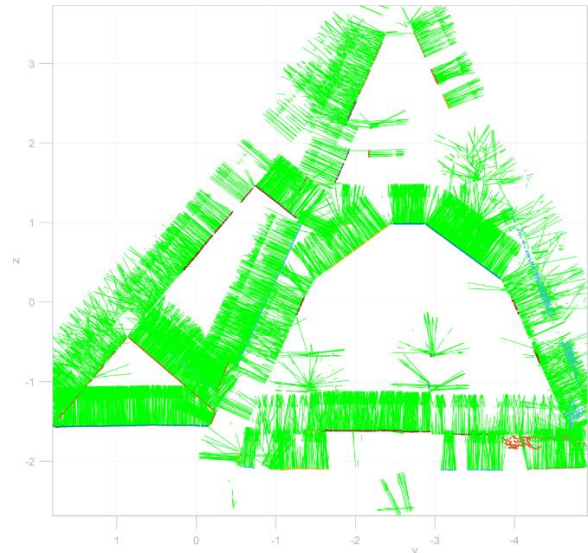


Figure 7: Normal vectors in a 2D slice of a pair of rafters.

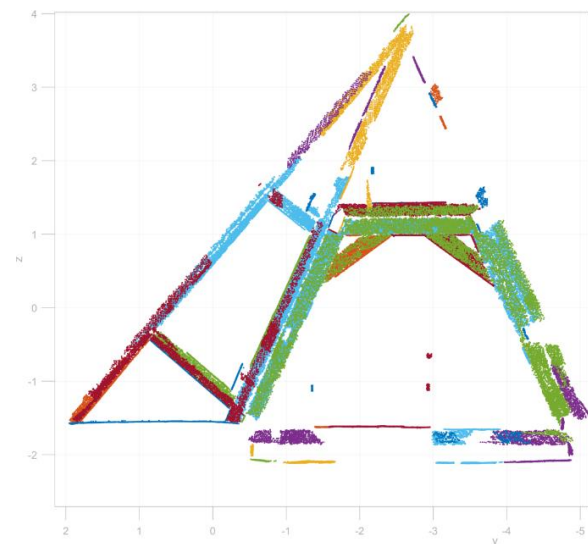


Figure 8: Segments of different beams; different colours represent different segment IDs.

To detect planar side faces of beams, region growing segmentation is used in the next step. The results in Fig. 8 were achieved with a maximum angle of 6° between the normal vectors of two neighbouring points as the homogeneity criterion and a search radius of 0.03 m. The figure shows, that some segments contain points on side faces of multiple beams. This systematic effect appears due to the selected local homogeneity criterion if the transition between the beams is sufficiently smooth. In some cases, gaps between elements or cracks in the wood may cause an otherwise smooth surface to be split up into two or more segments.

In the top of the roof, near the ridge, there is a noticeable reduction in the quality and completeness of the point cloud segmentation. One main reason for the deterioration of quality is scan shadows caused by the wooden walkways on both levels in the selected roof structures, as well as other installations in the roof. This quality issue is reflected in the results of the segmentation and affects the results throughout this workflow.

The classification and detection of segments that belong to the same wooden beam were discussed in the previous sections of this work. The resulting beams are visualised in Fig. 9 and Fig. 10. Whereas Fig. 9 consists of planar beam segments only (represented by the MBR), the beams in Fig. 10 are modelled with cuboids. Both figures show incomplete areas. While the automatically computed results in Fig. 9 show incomplete areas in the top of the roof, the results in Fig. 10 show a more complete model of intersected and elongated beams. The beams have been elongated semi-automatically with user guidance. In this step, two selected beams are elongated to their intersection point, if the length of their joint axis is less than 0.05 m. An automated validation of the beams with points of the laser scan is still missing.

Each step of the processing chain has been evaluated individually to determine appropriate parameter values. All parameters of the proposed workflow and their values are shown in Table 1. The set parameter values yield good results for the selected test datasets but might need some fine-tuning for other data.

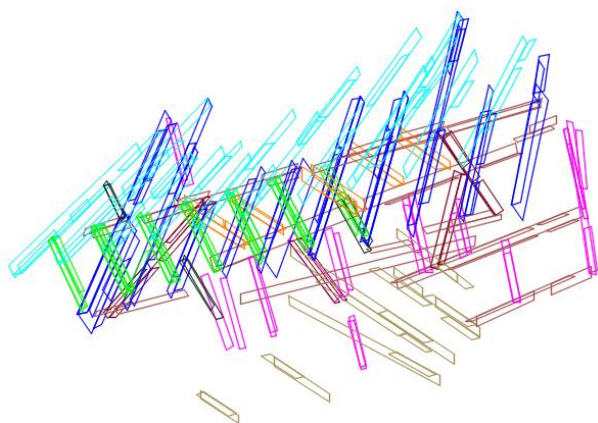


Figure 9: Adjacent beam segments are associated to describe a beam; different colours represent different roles in the structural system. The colouring was chosen manually for a better visual understanding.

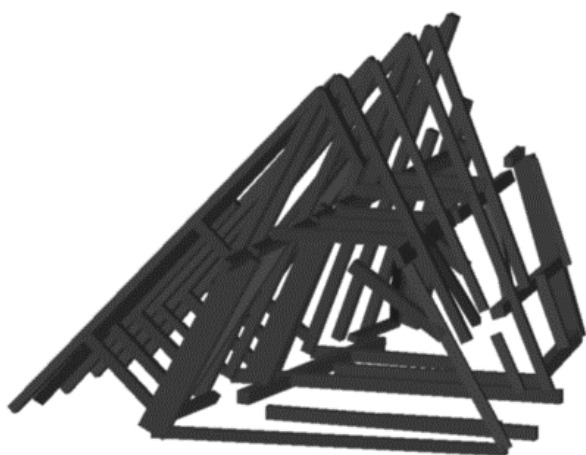


Figure 10: 3D model containing beams represented by cuboids.

Table 1: Summary of parameter values.

Processing step	Parameter	Value
opalsNormals	K-nearest neighbours	8
	Max. search radius	0.09 m
opalsSegmentation	Search radius	0.05 m
	α_{max} (1)	6.0 deg
Segment Classification	Segment planarity RMSE	0.04 m
	Min. beam width (w_{min})	0.4 m
	Max. beam width (w_{max})	0.1 m
Classification Beam segment (Fig. 5a)	Elongation factor (f_{elong})	> 5.0
	Area ratio (f_{area})	> 0.5
Classification Another segment (Fig. 5c)	Elongation factor (f_{elong})	< 4.5
	Area ratio (f_{area})	> 0.8
User-guided beam intersection	Max. joint axis length	0.05 m

4. Examples

All results shown in this article were obtained from 3D laser scanning datasets recorded with a Z+F Imager@ 5010C. Two selected datasets have been recorded in the roof of the Amalienburg in Vienna. The Amalienburg is part of the Vienna Imperial Palace complex. Dendrochronological analysis in the recorded wing of the Amalienburg determined that most of the used timber was felled in 1693/94 (Eßer *et al.*, 2016a)¹.

The first of two selected datasets of the Amalienburg, which was used in the previous figures, was captured from five different scan positions and contains approximately 3.5 million points. Typical point distances at the beam surface range from 1 mm to 1 cm. Since the dataset was taken from only five points of view, there are several scan shadow areas that have been scanned insufficiently. The result of the automatic beam reconstruction is shown in Fig. 10.

The second example was also taken from the same scan campaign in the Amalienburg. The used point cloud is a small section of the full scan campaign involving over 40 scan positions. The dataset consists of 2 million points and because of the many different scan positions, the point density is higher than in the previous dataset. The construction is in the very common form of a rafter roof with inclined principal trusses. Both levels of this construction contain wooden walkways including handrails, as shown in Fig. 11. The scan also contains the roof covering. The roof tiles have no relevance for the architectural and the structural model and need to be removed during processing. The results are shown in Fig. 12, and this dataset is used for further qualitative analysis.

The third dataset consists of a complete roof structure of the southern wing of the Austrian National Library. The Austrian National Library is also located in the Hofburg and was originally accommodating the Imperial Library. The scan was subsampled to 6 million points. The selected roof truss has a length of more than 40 m and a span width of approximately 25 m. The data and results are shown in Fig. 16. This dataset was used to investigate the computation time and demonstrate the ability to process a large dataset.

¹ The dendrochronological analysis was done by Dr. Michael Grabner, University of Natural Resources and Life Sciences, Vienna.

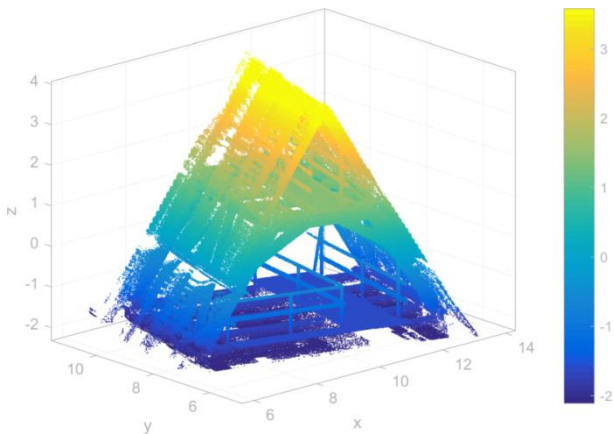


Figure 11: Point cloud of the roof construction in the Amalienburg, Vienna Imperial Palace.

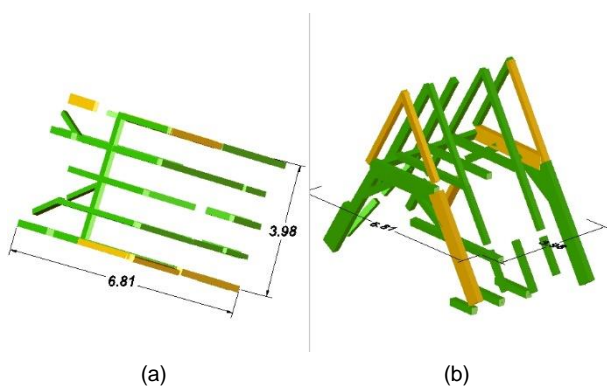


Figure 12: Automatically-reconstructed beams represented by their best fitting cuboids (colours show fitting accuracy):
a) Top view, and b) 3D view.

5. Discussion

As the sets of experiments show, the developed workflow is heavily dependent on the results of the segmentation shown in Fig. 13. For the chosen region growing with a comparison of normal vectors, no optimal homogeneity criterion could yet be found, whereby damages on the wood do not split up the element into multiple segments and gaps between two elements are identified as such and prevent faces of different beams being merged into one segment. However, the segmentation method can be changed and adapted easily within this workflow.

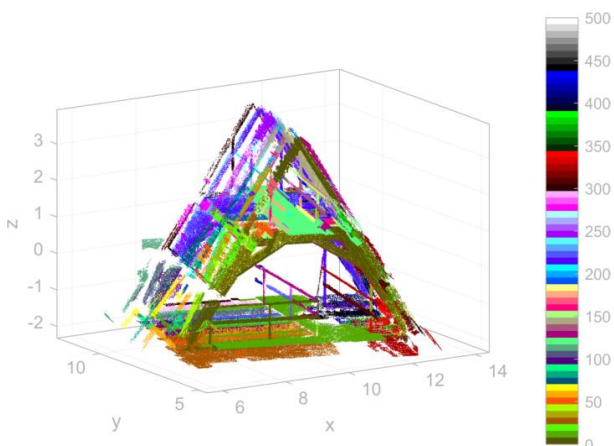


Figure 13: Results of the segmentation process.

Fig. 12 shows the top view and the 3D model of the roof construction containing the automatically-detected beams which are part of the structure. Beams with a σ_0 in the least squares fit smaller than 0.01 m are coloured green, beams with a σ_0 smaller than 0.025 m yellow. A visual analysis on the completeness of the result shows that 34 out of 40 beams present in the construction were at least partially detected. For a structural analysis, this model needs to be completed and expanded by the joints of the beams. An accuracy analysis has been carried out on the difference model between the point cloud and the reconstructed beams (Fig. 14).

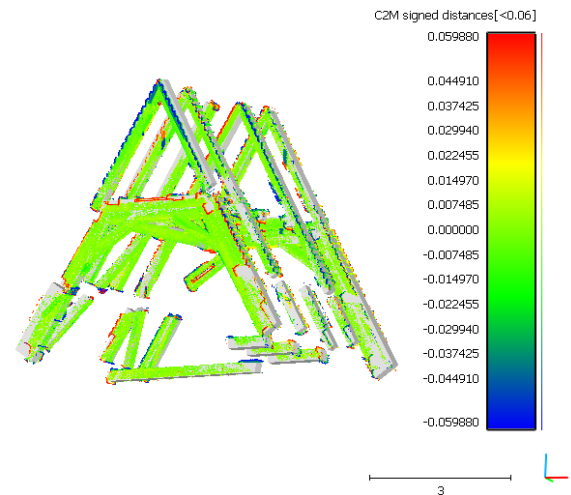


Figure 14: Accuracy analysis. The colour values of the points represent the distance from the modelled beams.

The colour values in Fig. 14 represent the signed distances from the points to the modelled beams, calculated with CloudCompare Cloud2Mesh-Distance. Only points with a maximum distance of ± 0.06 m to the modelled beams have been taken into account for the statistical analysis. As a result, points that are not on beams are included in the calculations if they are close enough –e.g. on the roof tiling or the wooden walkways. This has some negative impact on the statistics. The histogram in Fig. 15 shows a unimodal distribution of the signed distances between points and beams. The mean value of the absolute differences results in 9 mm and the standard deviation is 14 mm. For a more robust indication of accuracy, the median was calculated and results in 3 mm.

C2M signed distances[<0.06] (2000489 values) [256 classes]

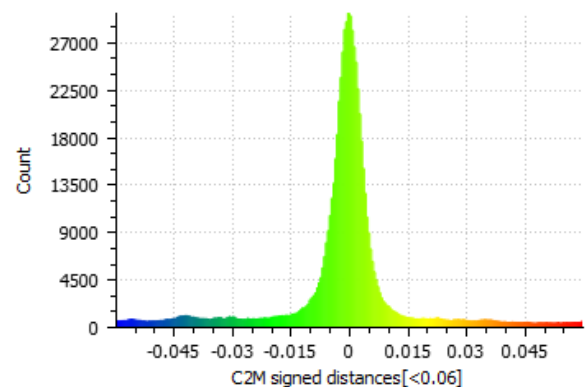


Figure 15: Histogram showing the distances (in meter) between point cloud and modelled beams.

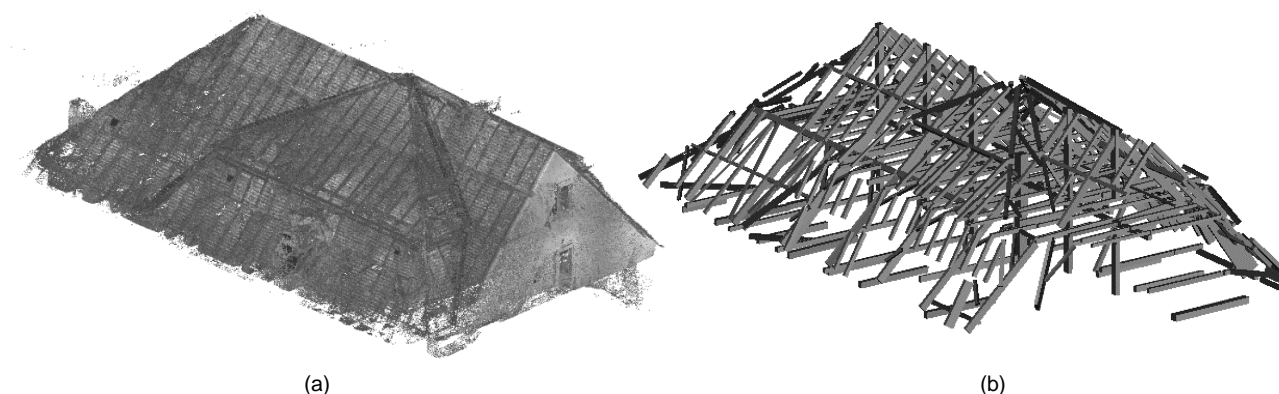


Figure 16: Historic roof structure of the southern wing of the National Library Vienna: a) Point cloud and b) computed beam model.

The deviations of beams from an ideal cuboid shape have not been analysed in detail yet, as we currently assume a high regularity. For irregular shapes different approaches should be considered in the future development: Tree reconstruction from point clouds generally involves elongated, but not straight objects (Thies, Pfeifer, Winterhalder, & Gorte, 2004; Raunonen, et al., 2013; Wang, Hollaus, Puttonen, & Pfeifer, 2016). Many approaches are based on the idea of following the form by advancing and adapting and moving a base model along the given point cloud. For modelling the irregular cross-section, splines or harmonic basis functions can be used to adapt to the deviation from an ideal cross-section shape (Pfeifer & Winterhalder, 2004; Wang, Kankare, Puttonen, Hollaus, & Pfeifer, 2016).

As part of the work, a runtime analysis was carried out. The program was therefore tested on a common business PC with an Intel® Core™2 Quad Processor Q8400 (4x 2.67 GHz) and 8 GB RAM. While the time complexity for the calculation of the normal vectors and the segmentation process is linear with the number of points and therefore approximated with $O(n)$, the runtime for the segment classification and the cuboid fit is also depending on the number of segments m and thus the complexity is approximately $O(n+m)$. The runtime was tested on both test datasets of the Amalienburg and on a scan of the roof of the Austrian National Library (Fig. 16).

Because of the lower point density in the subsampled National Library dataset, compared to the other test datasets, a bigger search radius of 6 cm was chosen for the segmentation. The results of the runtime analysis, shown in Table 2, confirm the theoretical complexity analysis.

The runtime analysis also shows that the computation time for bigger roof constructions, like the National Library, still takes several hours. This is partly because of the high number of points, but mainly due to the big number of beams in the construction. Yet, compared to the time consuming manual work steps, a considerable amount of time could already be saved.

When having a detailed look at the results, in some areas systematic errors occur, when two beams are (almost) parallel and close to each other. The question on how to handle those beams, where not enough points can be measured in the gap between to detect the beam side faces, remains unanswered.

Table 2: Runtime analysis

Computation	Dataset		
	Amalien-Burg 1 3577953 pts	Amalien-Burg 2 2000489 pts	National Library 6000000 pts
Normal vector calculation	0h 02" 21'	0h 01" 48'	0h 10" 42'
Segmentation	0h 06" 01'	0h 05" 57'	0h 09" 29'
No. of segments	1199	501	3210
Segment Classification	0h 13" 24'	0h 16" 32'	1h 02" 46'
No. of beam segments	344	205	1797
Cuboid Fitting	0h 08" 55'	0h 05" 25'	0h 38" 50'
No. of beams	71	36	463
Total Time	0h 30" 41'	0h 29" 42'	2h 01" 47'

6. Conclusion

The results, presented in the previous section, confirm that the proposed method for the reconstruction of historic timber structures is technically feasible. A high degree of automation for the modelling of beams is enabled by the detection of beam segments belonging to the same wooden beam. Only a few thresholds, such as the beam diameter or the search radius for the segmentation, need to be adjusted manually, in accordance with the data properties of the laser scans and the properties of the specific roof construction.

A trade-off between high point density and high performance has to be made. Lower point density (average point distances up to 1-2 cm) has only little effect on the quality of the final models, if the parameters of the normal vector computation and the segmentation can be adjusted properly. Very inhomogeneous point density, however, makes it difficult to find suitable parameters for an entire dataset. The quality issues regarding segmentation and further processing results lead to an incomplete automated detection of beams, which in turn requires an intense global analysis of the structure in order to produce a complete documentation of the construction. Several parameters such as the distance between rafters, ridge height, and beam dimension –as well as a catalogue of common joints in traditional timber

structures— need to be included in the automated analysis to produce a complete reconstruction result. One major aim is to model missing beams with the gained knowledge about the repetition of the rafters and patterns in the structure. To preserve the results to be based on the recorded points of the laser scan, beams that are reconstructed with overall knowledge need to be validated. A validation that requires at least some points of the point cloud on the surface of a reconstructed beam would ensure that no roof element, which has in fact been removed or replaced, is reconstructed by mistake.

With the information from the full 3D architectural model—including beam dimensions, axes of the beams and joints—it is possible to move on to the structural model. The used geometric model needs to be as complete as possible, since otherwise no reliable structural model can be derived. There will be weak points in the structure due to missing beams and joints. Furthermore, for a correct structural assessment, the question of how to deal with deformations or non-cuboid shape of beams is yet to be

solved. In general, this modelling of structural and architectural information from the same 3D point cloud permits interdisciplinary documentation and analysis of historic timber structures, where photogrammetry provides various methods of data processing, and architects and civil engineers can contribute their expert knowledge on the structure of historic roofs. Up-to-date structural engineering software respects nonlinear structural behaviour of constructions taking into account aspects such as material characteristics, joint behaviour for different kinds of loads and cracking sequences, etc. (Eßer et al., 2016a).

A future aim for this work could be to store the information in Building Information Models (BIM), enabling efficient collaboration in adaptive re-use planning between the various disciplines involved. Bringing point cloud data to BIM is already an ongoing research topic and development process in the field of building and planning in existing structures, where software solutions are still required.

References

- Attene, M., & Spagnuolo, M. (2000). Automatic surface reconstruction from point sets in space. *Computer Graphics Forum*, 19(3), 457–465. doi:10.1111/1467-8659.00438
- Baik, A., Yaagoubi, R., & Boehm, J. (2015). Integration of Jeddah historical BIM and 3D GIS for documentation and restoration of historical monument. *The International Archives of Photogrammetry, Remote Sensing and Spatial Information Sciences*, XL-5/W7, 29–34. doi:10.5194/isprsarchives-XL-5-W7-29-2015
- Bassier, M., Hadjidemetriou, G., Vergauwen, M., Van Roy, N., & Verstrynghe, E. (2016). Implementation of Scan-to-BIM and FEM for the Documentation and Analysis of Heritage Timber Roof Structures. In M. Ioannides, E. Fink, A. Moropoulou, M. Hagedorn-Saupe, A. Fresa, G. Liestøl, . . . P. Grussenmeyer (Ed.), *Digital Heritage. Progress in Cultural Heritage: Documentation, Preservation, and Protection. EuroMed 2016* (pp. 79–90). Springer, Cham. doi:10.1007/978-3-319-48496-9_7
- Besl, P., & McKay, N. (1992). A method for registration of 3D Shapes. *IEEE Transactions on Pattern Analysis and Machine Intelligence*, 14, 239–254. doi:10.1109/34.121791
- Chida, A., & Masuda, H. (2016). Reconstruction of polygonal prisms from point-clouds of engineering facilities. *Journal of Computational Design and Engineering*, 3(4), 322–329. doi:10.1016/j.jcde.2016.05.003
- Dore, C., & Murphy, M. (2017). Current state of the art historic building information modelling. *International Archives of Photogrammetry, Remote Sensing and Spatial Information Sciences*, XLII-2/W5, 185–192. doi:10.5194/isprs-archives-XLII-2-W5-185-2017
- Dorning, P., Nothegger, C., & Rasztovits, S. (2013). Efficient 3-D documentation of Neptune fountain in the park of Schönbrunn palace at millimeter scale. *Proceedings XXIV International CIPA Symposium, ISPRS Annals*, II, 5/W1, 103–108. doi:10.5194/isprsannals-II-5-W1-103-2013
- Eßer, G., Styhler-Aydın, G., & Hochreiner, G. (2016a). Construction history and structural assessment of historic roofs – An interdisciplinary approach. In K. Van Balen, & E. Verstrynghe (Eds.), *Structural analysis of historical constructions. Anamnesis, diagnosis, therapy, controls* (pp. 790–795). London, GB.
- Eßer, G., Styhler-Aydın, G., & Hochreiner, G. (2016b). The historic roof structures of the Vienna Hofburg: An innovative interdisciplinary approach in architectural sciences laying ground for structural modeling. In J. Eberhardsteiner, W. Winter, A. Fadaï, & M. Pöll (Eds.), *WCTE 2016. World conference on timber engineering* (pp. 3039–3047). Wien, Austria.
- Fischler, M., & Bolles, R. (1981). Random sample consensus: a paradigm for model fitting with applications to image analysis and automated cartography. *Communications of the ACM*, 24(6), 381–395. doi:10.1145/358669.358692
- Glira, P., Pfeifer, N., Briese, C., & Ressel, C. (2015). A Correspondence Framework for ALS Strip Adjustments based on Variants of the ICP Algorithm. *Photogrammetrie, Fernerkundung, Geoinformation*, 4, 275–289. doi:10.1127/pfg/2015/0270

- Hochreiner, G., Eßer, G., & Styhler-Aydın, G. (2016). Modern timber engineering methods in the context of historical timber structures. In J. Eberhardsteiner, W. Winter, A. Fadaei, & M. Pöll (Eds.), *WCTE 2016. World conference on timber engineering* (pp. 4830–4838). Wien, Austria.
- Hoppe, H., DeRose, T., Duchamp, T., McDonald, J., & Stuetzle, W. (1992). Surface reconstruction from unorganized points. *SIGGRAPH '92 Proceedings of the 19th annual conference on Computer graphics and interactive techniques. ACM SIGGRAPH Computer Graphics*, 26(2), 71–78. doi:10.1145/142920.134011
- International Organization for Standardization. (2016). Industrial automation systems and integration – Product data representation and exchange – Part 21: Implementation methods: Clear text encoding of the exchange structure. *ISO/DIS Standard No. 10303-21*. Retrieved from <https://www.iso.org/standard/63141.html>.
- Jung, J., Hong, S., Jeong, S., Kim, S., Cho, H., Hong, S., & Heo, J. (2014). Productive modeling for development of as-built BIM of existing indoor structures. *Automation in Construction*, 42, 68–77. doi:10.1016/j.autcon.2014.02.021
- Kazhdan, M., Bolitho, M., & Hoppe, H. (2006). Poisson surface reconstruction. *Symposium on Geometry Processing* (pp. 61–70). The Eurographics Association. doi:10.2312/SGP/SGP06/061-070
- Lee, J., Son, H., Kim, C., & Kim, C. (2013). Skeleton-based 3-D reconstruction of as-built pipelines from laser-scan data. *Automation in Reconstruction*, 35, 199–207. doi:10.1061/9780784412343.0031
- Li, W., Goodchild, M., & Church, R. (2013). An efficient measure of compactness for two-dimensional shapes and its application in regionalization problems. *International Journal of Geographical Information Science*, 1227–1250. doi:10.1080/13658816.2012.752093
- Nothegger, C., & Dorninger, P. (2009). 3D filtering of high-resolution terrestrial laser scanner point clouds for cultural heritage documentation. *Photogrammetrie, Fernerkundung, Geoinformation*, 1, 53–63. doi:10.1127/0935-1221/2009/0006
- Pfeifer, N., & Winterhalder, D. (2004). Modelling of tree cross sections from terrestrial laser scanning data with free-form curves. *International Archives of Photogrammetry, Remote Sensing and Spatial Information Sciences*, 36(8/W2), 76–81.
- Pfeifer, N., Mandlbürger, G., Otepka, J., & Karel, W. (2014). OPALS – A framework for Airborne Laser Scanning data analysis. *Computers, Environment and Urban Systems*, 45, 125–136. doi:10.1016/j.compenvurbsys.2013.11.002
- Pöchtrager, M., Styhler-Aydın, G., Döring-Williams, M., & Pfeifer, N. (2017). Automated Reconstruction of Historic Roof Structures from Point Clouds – Development and Examples. *ISPRS Ann. Photogramm. Remote Sens. Spatial Inf. Sci.*, IV-2-W2, 195–202. doi:10.5194/isprs-annals-IV-2-W2-195-2017
- Rabbani, T., Dijkman, S., Van den Heuvel, F., & Vosselman, G. (2007). An integrated approach for modelling and global registration of point clouds. *ISPRS Journal of Photogrammetry and Remote Sensing*, 61(6), 355–370. doi:10.1016/j.isprsjprs.2006.09.006
- Raumonen, P., Kaasalainen, M., Åkerblom, M., Kaasalainen, S., Kaartinen, H., Vastaranta, M., ... Lewis, P. (2013). Fast automatic precision tree models from terrestrial laser scanner data. *Remote Sensing*, 5(2), 491–520. doi:10.3390/rs5020491
- Stylianidis, E., & Remondino, F. (2016). *3D Recording, Documentation and Management of Cultural Heritage*. Caithness, UK: Whittles Publishing.
- Thies, M., Pfeifer, N., Winterhalder, D., & Gorte, B. (2004). Three-dimensional reconstruction of stems for assessment of taper, sweep and lean based on laser scanning of standing trees. *Scandinavian Journal of Forest Research*, 19(6), 571–581. doi:10.1080/02827580410019562
- Thomson, C., & Boehm, J. (2015). Automatic geometry generation from point clouds for BIM. *Remote Sensing*, 7(9), 11753–11775. doi:10.3390/rs70911753
- Vosselman, G., & Maas, H.-G. (2010). *Airborne and Terrestrial Laser Scanning*. Caithness, UK: Whittles Publishing.
- Wang, D., Hollaus, M., Puttonen, E., & Pfeifer, N. (2016). Automatic and self-adaptive stem reconstruction in landslide-affected forests. *Remote Sensing*, 8(12), p. 974. doi:10.3390/rs8120974
- Wang, D., Kankare, V., Puttonen, E., Hollaus, M., & Pfeifer, N. (2016). Reconstructing stem cross section shapes from terrestrial laser scanning. *IEEE Geoscience and Remote Sensing Letters*, 14(2), 272–276. doi:10.1109/LGRS.2016.2638738
- Xiong, X., Adan, A., Akinci, B., & Huber, D. (2013). Automatic creation of semantically rich 3D building models from laser scanner data. *Automation in Construction*, 31, S. 325–337. doi:10.1016/j.autcon.2012.10.006

DIGITAL RECONSTRUCTION OF HISTORIC ROOF STRUCTURES: DEVELOPING A WORKFLOW FOR A HIGHLY
AUTOMATED ANALYSIS

- Yang, X., Koehl, M., & Grussenmeyer, P. (2017). Parametric modelling of as-built beam framed structure in BIM environment. *International Archives of Photogrammetry, Remote Sensing and Spatial Information Sciences, XLII-2/W3*, 651–657. doi:[10.5194/isprs-archives-XLII-2-W3-651-2017](https://doi.org/10.5194/isprs-archives-XLII-2-W3-651-2017)
- Zhang, R., & Zakhor, A. (2014). Automatic identification of window regions on indoor point clouds using LiDAR and cameras. *Applications of Computer Vision (WACV), 2014 IEEE Winter Conference*, 107–114. doi:[10.1109/WACV.2014.6836112](https://doi.org/10.1109/WACV.2014.6836112)